JOURNAL OF SYNCHROTRON RADIATION
ISSN 1600-5775

# Investigation of the multiplet features of $SrTiO_3$ in X-ray absorption spectra based on configuration interaction calculations

M. Wu,[a] Houlin L. Xin,[b] J. O. Wang,[c] X. J. Li,[a] X. B. Yuan,[a] H. Zeng,[a] J.-C. Zheng[a,d]* and H.-Q. Wang[a,d]*

[a]Fujian Provincial Key Laboratory of Semiconductors and Applications, Collaborative Innovation Center for Optoelectronic Semiconductors and Efficient Devices, Department of Physics, Xiamen University, Xiamen 361005, People's Republic of China, [b]Center for Functional Nanomaterials, Brookhaven National Laboratory, Upton, NY 11973, USA, [c]Beijing Synchrotron Radiation Facility, Institute of High Energy Physics, Chinese Academy of Sciences, Beijing 100049, People's Republic of China, and [d]Xiamen University Malaysia, 439000 Sepang, Selangor, Malaysia.
*Correspondence e-mail: jczheng@xmu.edu.cn, hqwang@xmu.edu.cn

Received 11 January 2018
Accepted 12 March 2018

Edited by R. W. Strange, University of Essex, UK

**Keywords:** soft X-ray absorption; configuration interaction cluster calculation; 3*d* transition metal oxide; crystal field effect.

Synchrotron-based $L_{2,3}$-edge absorption spectra show strong sensitivities to the local electronic structure and chemical environment. However, detailed physical information cannot be extracted easily without computational aids. Here, using the experimental Ti $L_{2,3}$-edges absorption spectrum of $SrTiO_3$ as a fingerprint and considering full multiplet effects, calculations yield different energy parameters characterizing local ground state properties. The peak splitting and intensity ratios of the $L_3$ and $L_2$ set of peaks are carefully analyzed quantitatively, giving rise to a small hybridization energy around 1.2 eV, and the different hybridization energy values reported in the literature are further addressed. Finally, absorption spectra with different linearly polarized photons under various tetragonal crystal fields are investigated, revealing a non-linear orbital–lattice interaction, and a theoretical guidance for material engineering of $SrTiO_3$-based thin films and heterostructures is offered. Detailed analysis of spectrum shifts with different tetragonal crystal fields suggests that the $e_g$ crystal field splitting is a necessary parameter for a thorough analysis of the spectra, even though it is not relevant for the ground state properties.

## 1. Introduction

$SrTiO_3$ (STO) compound has attracted longstanding attention due to its fascinating properties both for fundamental research and applications in functional oxide electronics (Cen *et al.*, 2009; Choi *et al.*, 2009), as well as in the field of renewable energy (Marschall, 2014; Comes *et al.*, 2015). Bulk STO, $Ti^{4+}$ with $3d^0$ electronic configuration, has a perovskite crystal structure with a cubic lattice constant of 3.905 Å. It is usually used as a substrate in thin-film engineering due to its structural and chemical compatibility with other perovskite transition metal oxides (Schlom *et al.*, 2007). STO bulk and related thin films show novel physical properties: for instance, the quantum paraelectric and the incipient ferroelectrics at the surfaces and heterostructures of STO (Haeni *et al.*, 2004; Dawber *et al.*, 2005); the high mobility of two-dimensional electron gas exhibiting quantum oscillations in magneto-transport measurements at the interfaces of $LaAlO_3$–STO heterostructures (Ohtomo & Hwang, 2004; Hwang *et al.*, 2012); the unexpected superconductivity at $T_c$ = 0.2 K at the interface between $LaAlO_3$ and STO (Reyren *et al.*, 2007), *etc.*

Synchrotron radiation soft X-ray absorption measurements for 3*d* transition metal compounds ($L_{2,3}$-edges, typically with

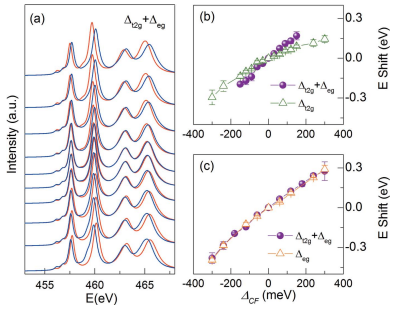

photon energies in the 400–1000 eV range) are sensitive to the local valence state, orbital occupation and spin arrangement, which is important for exploring the correlated interactions among different degrees of freedom, *e.g.* charge, spin, orbital, lattice, *etc*. However, detailed structural and electronic information cannot be extracted from the $L_{2,3}$-edge absorption spectrum without computational aids. Density functional theory (DFT) is highly desirable but has been a longstanding theoretical challenge due to strong multiplet effects such that the spectral function calculated from first principles fails.

The soft X-ray absorption spectrum of single-crystal STO shows no exception, where the intensity ratios at the Ti $L_{2,3}$-edges are still under debate. For instance, the theoretical spectra of STO bulk and thin films based on DFT can reproduce well the peak energy positions and the polarization-dependent peak shifts for STO thin films, but the spectra show opposite tendencies for the peak intensities of the $L_3$ set of peaks (Woicik *et al.*, 2007). Further, spectra calculated by DFT in the independent particle approximation taking three different types of one-electron potentials into account all give incorrect peak intensities (Krüger, 2010). Many calculation approaches have been developed over the last decades to try to understand the $L_{2,3}$-edge absorption spectrum: for example, time-dependent DFT, which to our knowledge has not been applied to STO but to other $3d^0$ oxides such as $V_2O_5$ (Fronzoni *et al.*, 2012) and $FeTiO_3$ (Bunău & Joly, 2012) with fairly good agreements with experimental absorption spectra; the Bethe–Salpeter equation, where the theoretical spectra either lack capturing of the peak intensities at the STO Ti $L_{2,3}$-edges (Laskowski & Blaha, 2010; Gilmore *et al.*, 2015) or exhibit an incorrect peak splitting between the leading peaks and the excitation peaks (Gilmore *et al.*, 2015; Vinson *et al.*, 2011); multichannel multiple-scattering calculations, where the calculated spectra show variations in relative peak splitting compared with the experimental STO spectrum (Krüger, 2010; Krüger & Natoli, 2016); and *ab initio* full multiplet calculations (Ikeno *et al.*, 2009; Haverkort *et al.*, 2012; Ramanantoanina & Daul, 2017), where the Ti $L_{2,3}$-edges show a better description of the experimental spectrum in terms of relative peak positions and intensities. We note that all of these approaches can reproduce the STO Ti $L_{2,3}$ absorption spectrum reasonably well but demand large computational efforts which shows the advantages of understanding the spectrum of large electron systems. Furthermore, none has heretofore quantitatively accounted for the variation of the intensity ratios, which will be mainly addressed in the present work.

For the STO of interest here, the $L_{2,3}$ spectrum can also be reproduced well using configuration interaction (CI) cluster calculations and a regular PC. For instance, de Groot *et al.* reported a detailed calculation of the $L_{2,3}$-absorption spectrum for $d^0$ compounds including $K^+$, $Ca^{2+}$, $Sc^{3+}$ and $Ti^{4+}$ in octahedral symmetry (de Groot *et al.*, 1990). Tanaka & Jo reported the calculated resonant photoemission spectra for different $3d$ compounds, including the $TiO_2$ $L_{2,3}$-absorption spectrum as a $3d^0$ compound example (Tanaka & Jo, 1994). Bocquet *et al.* performed CI calculations for a wide range of early transition metal compounds by analyzing the core-level X-ray photoemission spectra (Bocquet *et al.*, 1996). Kroll *et al.* reported the final-state projection method based on CI which allows separation of the charge transfer effect on each possible final-state configuration taking the explicit STO $L_{2,3}$-absorption spectrum as the model system (Kroll *et al.*, 2015). We note that the Ti $L_{2,3}$-absorption spectrum shows sensitivities to small structural and electronic variations so that different fine structures appear in anatase and rutile $TiO_2$ (Maganas *et al.*, 2014), $BaTiO_3$ (Ootsuki *et al.*, 2014), $PbTiO_3$ (Torres-Pardo *et al.*, 2011), $PbZr_{0.2}Ti_{0.8}O_3$ (Arenholz *et al.*, 2010) and STO (Uehara *et al.*, 1997) as well as their thin films with lower symmetries. Moreover, none of the above CI calculations are specialized for STO compound or solving the debate regarding the intensity ratios at the Ti $L_{2,3}$-edges.

We therefore aim to provide a comprehensive understanding of the multiplet structures and the local ground state properties of STO compound. In particular, we analyze the intensity ratios quantitatively based on CI cluster calculations. In combination with our previous studies of $LaTiO_3$ compound with a $TiO_6$ cluster of $3d^1$ electronic configuration (Wu *et al.*, 2017), our present calculations provide a comparison between $LaTiO_3$ and STO compounds. These detailed studies of the absorption spectra with different valence states also offer the potential to understand the interfacial physics of the heterostructure composed of $LaTi^{3+}O_3$ and $ST^{4+}O$ and the ground state of the $(La,Sr)TiO_3$ bulk solid solution. Furthermore, we present the photon polarization-dependent absorption spectra with different tetragonal crystal fields, relating the linear dichroic spectrum to the character of the $d$ states and the local electronic structures. This study reveals the orbital–lattice interactions of the system and provides guidance for the experimental design in strain engineering of STO-based thin films and heterostructures. Nevertheless, cluster calculations are proposed to reproduce and to help understand the experimental spectra, which will provide a variety of energy parameters representing the ground state properties. CI cluster calculations are thus complementary and verify other calculations.

In the following we introduce simple principles of CI cluster calculations in §2. In §3, we start from a direct comparison between the simulated spectrum and the experimentally measured STO Ti $L_{2,3}$-edges absorption spectrum. In §3.2, we investigate the effect of different energy parameters on multiplet structures. In particular, we analyze the peak splitting and peak intensity ratios at the Ti $L_{2,3}$-edges which give rise to the crystal field splitting energy $10Dq$ and hybridization strength $pd\sigma$ values. In §3.3, we focus on the photon polarization-dependent absorption spectra with different tetragonal crystal fields. A conclusion is given §4.

## 2. CI cluster calculation

The theory for CI cluster calculations of transition metal compounds was developed from ligand field calculations taking the full multiplet effects into account (Haverkort *et al.*, 2012; van der Laan *et al.*, 1981, 1986; Haverkort, 2016),

showing the advantages of interpreting the $L_{2,3}$-edges excitation spectrum over the last decades. Each calculation is carried out using the following procedure: a many-electron configuration basis is firstly built for the initial and the final state separately. We concern only the three lowest energy configurations in our present calculations. The Hamiltonian matrix comprises different energy parameters, including the crystal field of 3*d* orbitals, the crystal field of ligand *p* orbitals, the hopping term and the Coulomb interaction plus the charge transfer energy term for the initial-state Hamiltonian. The final-state Hamiltonian takes into account the attractive interaction $U_{pd}$ between the core hole and the 3*d* electron as well as spin–orbit coupling effects. Finally, the transition probability is calculated for each final state from a given initial state with an authorized incident photon polarization based on Fermi's Golden rule with the electron dipole approximation. Regarding the general background and details on performing the CI cluster calculations, refer to the literature mentioned above.

## 3. Results and discussions

### 3.1. Comparison with experiment

We measured the $L_{2,3}$-edges X-ray absorption spectrum for a STO single-crystal at beamline 4B9B of the Beijing Synchrotron Radiation Facility. The spectrum was measured in total electron yield mode, as shown in Fig. 1. The experimental spectrum comprises two leading peaks which are typical for $3d^0$ compounds, and the $L_3$, $L_2$ set of peaks owing to the spin–orbit coupling of the Ti 2*p* levels. We denote the $L_3$ and $L_2$ absorption peaks as $a_1(E = 457.6\ \text{eV})$, $a_2(E = 459.9\ \text{eV})$, $b_1(E = 462.9\ \text{eV})$ and $b_2(E = 465.3\ \text{eV})$, corresponding to excitations of the form $2p_{j=3/2} \rightarrow t_{2g}$, $2p_{j=3/2} \rightarrow e_g$, $2p_{j=1/2} \rightarrow t_{2g}$ and $2p_{j=1/2} \rightarrow e_g$, respectively. One electron picture without taking the electron–electron correlations into account would provide the intensity ratio $I(a_1):I(a_2):I(b_1):I(b_2) = 6:4:3:2$ by considering the intensity ratio of 4:2 from excitations of, respectively, $2p_{j=3/2}$ and $2p_{j=1/2}$ levels and the intensity ratio of 6:4 between excitations to, respectively, $t_{2g}$ and $e_g$ states, which are obviously unresolved from experimental measurement. This indicates that the multipet features in the absorption spectrum are complicated and related to combined covalent effects and Coulomb interactions. We denote the intensity ratios of the $L_3$ and $L_2$ set of peaks as $I_{L3} = I(a_2)/I(a_1) = 1.1 \pm 0.05$ and $I_{L2} = I(b_2)/I(b_1) = 1.5 \pm 0.1$. The intensity of each peak is obtained by fitting the multiple peaks with Lorentzian profiles. Furthermore, from the energy position of the absorption peaks in the experimental spectrum, we obtain the energy splitting between the $L_3$ and $L_2$ set of peaks, *i.e.* $\Delta_{L3} = E(a_2) - E(a_1) = 2.3$ eV and $\Delta_{L2} = E(b_2) - E(b_1) = 2.4$ eV. The X-ray absorption spectra contain unique features and thus are usually used as a fingerprint for the ground state properties. Here, both the $\Delta_{L3,2}$ and $I_{L3,2}$ values at the $L_3$- and $L_2$-edges serve as good quantities for testing the multiplet effects and to confirm the energy parameters of our calculations, as will be discussed in detail below.

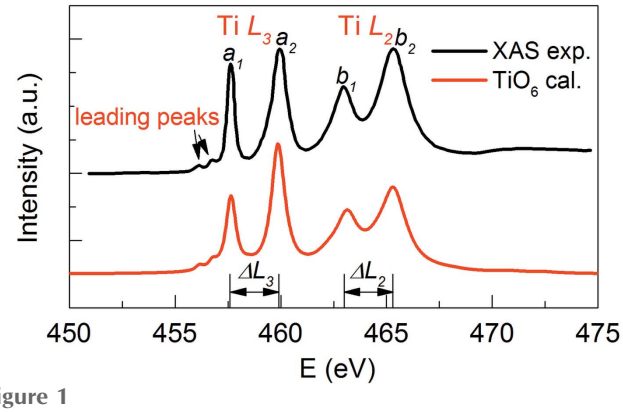


**Figure 1**
Comparison between the experimental X-ray absorption spectrum for a STO single-crystal (miscut angle < 0.05°, purchased from Crystec) and the calculated spectrum of STO (bottom).

We carried out CI cluster calculations for a $TiO_6$ cluster with $3d^0$ electronic configuration. The simulated spectrum shown in Fig. 1 is calculated with optimized parameters which can reproduce the experimental spectrum well. The parameters for the present calculations are (in units of eV): $U_{dd} = 6.0$, $U_{pd} = 8.0$, $\Delta = 6.0$, $10Dq = 1.8$ and $pd\sigma = -1.2$. We will discuss the magnitudes of these energy parameters and their effects on the multiplet structure in the next section.

### 3.2. Effects on the multiplet structures

In this section, we vary each energy parameter separately, while keeping the others at the optimized values as mentioned above, which could help in understanding the effect of each energy parameter on the multiplet structures. The multipole interactions of the Coulomb interaction are treated with the Hartree–Fock approximation where the radial wavefunctions are related to different Slater parameters, *i.e.* $F^2_{dd}$, $F^4_{dd}$ Slater parameters for *d*–*d* interactions and $F^2_{pd}$, $G^1_{pd}$, $G^3_{pd}$ Slater parameters for *p*–*d* interactions. Fig. 2(*a*) shows the simulated absorption spectra calculated with different Slater parameters. The Slater parameters are rescaled to 0%, 25%, 50%, 60%, 70%, 80%, 90% and 100% for the top to the bottom spectra which show dramatic differences. The absorption spectrum with 0% scaling factor corresponds to a single-particle scenario while that with 100% scaling factor corresponds to the spectrum for a free ion. Spectra with a scaling factor of less than 100% indicate the existence of the covalent screening and therefore the intra-atomic interactions of the solid state are considered. As shown in Fig. 2(*a*), the two leading peaks only exist if one considers a strong solid effect, *i.e.* values of the Slater integrals larger than 50% of the ionic values. Furthermore, the reductions of the Slater parameters not only reduce the relative intensities for excitations to $e_g$ levels and shift to $t_{2g}$ levels but also shift the leading peaks closer to the rest of the spectra, which is consistent with the decreasing intra-atomic interactions. We use the energy splitting between the leading peaks and the rest of the excitation peaks to determine the Slater parameters, which suggests a correction of 70–80% of the Slater parameters for the best agreement

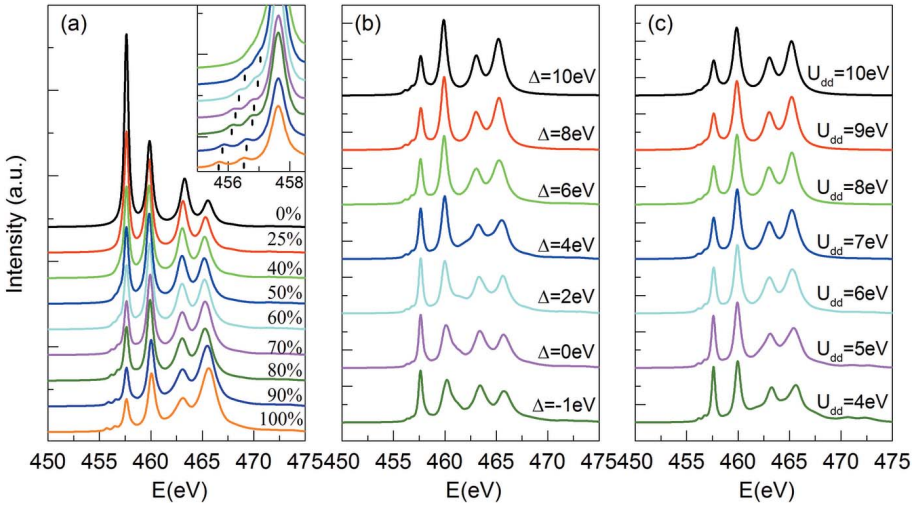


**Figure 2**
(*a*) Simulated absorption spectra for a $TiO_6$ cluster with different Slater parameters. Each subsequent spectrum has the value of the Slater integrals further rescaled by 0, 25, 40, 50, 60, 70, 80, 90 and 100% from top to bottom. The inset shows an enlarged plot of the two leading peaks regions. (*b*) Calculated isotropic spectra for different Δ from −1 to 10 eV. (*c*) The effect of *d*–*d* Coulomb interaction energy $U_{dd}$ from 4 to 10 eV on the simulated isotropic spectra. All spectra are shifted to the same first excitation peak (peak $a_1$ shown in Fig. 1).

with the experimental results. This correction factor is consistent with the value pointed out by de Groot *et al.* to account for the intra-atomic configuration interaction inside a solid (de Groot *et al.*, 1990). Finally, we note that the small leading peaks keep their intensities and energy splitting almost constant when varying other energy parameters, *e.g.* the charge transfer energy Δ and Coulomb interaction $U_{dd}$ as shown in Figs. 2(*b*)–2(*c*), as well as the crystal field splitting energy $10Dq$ in Fig. 3, which are shown as general small leading peaks in X-ray absorption spectra for $d^0$ compounds.

Figs. 2(*b*) and 2(*c*) show the simulated absorption spectra with different charge transfer energy Δ ranging from −1 eV to 10 eV and on-site electron–electron Coulomb interaction energy $U_{dd}$ from 4 eV to 10 eV, both of which characterize the energy differences among different electronic configuration bases. We note a contraction of the multiplet structures as Δ or $U_{dd}$ increases. However, the differences among the simulated spectra are small for Δ above 4 eV as well as for $U_{dd}$ values above 5 eV. Our simulations thus are insensitive to the Δ and $U_{dd}$ values, similar to the large uncertainties of Δ and $U_{dd}$ values reported by Haverkort *et al.* (2012), Tanaka & Jo (1994) or Bocquet *et al.* (1996). In the present calculations, we use the typical values $U_{dd}$ = 6.0, Δ = 6.0 for STO compound.

The crystal field effect is treated in a mean-field approximation and directly reflects the symmetry of the ground states. Fig. 3 shows the absorption spectra calculated with different crystal field splitting $10Dq$ values for the $TiO_6$ octahedron with cubic $O_h$ symmetry. The $L_3$- and $L_2$-absorption edges split into two peaks as $10Dq$ increases, which is often imaged as a splitting of the $L_3$- and $L_2$-edges into $t_{2g}$ and $e_g$ levels. One might expect that the energy difference between the $t_{2g}$ and $e_g$ levels is equal to the crystal field splitting energy $10Dq$ intuitively. Fig. 3(*b*) shows the averaged energy splitting between the $L_3$ set of peaks, *i.e.* $\Delta_{L3}$ as a function of $10Dq$ ($\Delta_{L2}$ is within the error bar), which obviously deviates from the grey dashed line representing the same magnitudes between the peak energy splitting $\Delta_{L3}$ and $10Dq$. The black dash-dot line represents the peak splitting $\Delta_{L3}$ and $\Delta_{L2}$ *versus* $10Dq$ which is reproduced from de Groot *et al.* with CI calculations for $3d^0$ compounds in general (de Groot *et al.*, 1990). Both curves show very similar tendencies but small derivations which might be related to the optimization of other energy parameters in the present calculations. A comparison of $\Delta_{L3}$ = 2.3 eV and $\Delta_{L2}$ = 2.4 eV from the experimental spectrum suggests a crystal field splitting energy $10Dq$ = 1.8–2.0 eV from our calculations, which is consistent with other CI calculations performed for STO compound. Fig. 3(*c*) shows the relative intensities of each peak separately. The peak intensities show no clear correlation, indicating that the emerged peaks as $10Dq$ switched on cannot be visualized as the splitting of atomic lines into two but as a multiplet effect, *i.e.* a redistribution of peak intensities over all lines.

In CI-based cluster calculations, the hopping term has been taken into account which enters the off-diagonal terms of the Hamiltonian and describes the hybridization strength between the transition metal ion and oxygen. The hopping term is expressed using the Slater–Koster parameters $pd\sigma$ and $pd\pi$, with $pd\sigma/pd\pi = -2.17$ reflecting the anisotropic hybridization

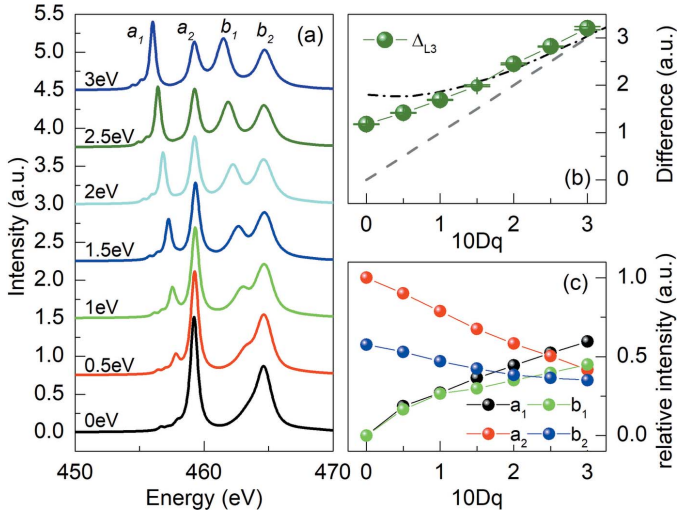


**Figure 3**
(*a*) Isotropic spectra with different crystal field splitting energies. (*b*) Energy splitting $\Delta_{L3}$ as a function of $10Dq$. The grey dashed line corresponds to the condition that the peak energy splitting $\Delta_{L3}$ is equal to $10Dq$. The black dot-dash line is reproduced from de Groot *et al.* (1990). (*c*) Relative intensities of different excitation peaks $a_1$, $a_2$, $b_1$ and $b_2$ *versus* $10Dq$ values. The intensities are normalized by $a_2$ peak intensity calculated at $10Dq$ = 0 eV.

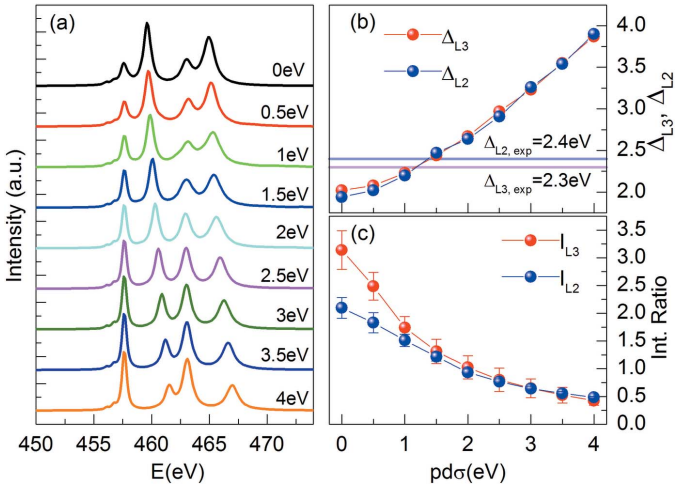


**Figure 4**
Isotropic spectra with different hybridization strengths. The effect of hybridization strength $pd\sigma$ (ranging from 0 to 4 eV with an interval of 0.5 eV) on the simulated isotropic spectra [(*a*)]. (*b*) Energy splitting $\Delta_{L3}$ and $\Delta_{L2}$ *versus* $pd\sigma$ values. The straight lines denote the experimental $\Delta_{L3,exp}$ and $\Delta_{L2,exp}$ values. (*c*) Calculated intensity ratio $I_{L3}$ and $I_{L2}$ as a function of different $pd\sigma$ values.

strengths (Bocquet *et al.*, 1996; Slater & Koster, 1954). Fig. 4(*a*) shows the effect of hybridization strength $pd\sigma$ ranging from 0 to 4 eV on the simulated isotropic spectra, which causes dramatic changes in the absorption spectra including the energy splitting between the $L_3$ and $L_2$ set of peaks, as well as the redistributions of peak intensities. The energy splitting $\Delta_{L3}$ and $\Delta_{L2}$ exhibit a monotonically increase as $pd\sigma$ increases (Fig. 4*b*), which agrees well with the theoretical prediction of the increasing energy splitting as hybridization increases by solving the determinant of the Hamiltonian (Bocquet *et al.*, 1996; Okada *et al.*, 1994). A further comparison between the experimental $\Delta_{L3}$ and $\Delta_{L2}$ values and the theoretical values suggests that $pd\sigma$ is in the energy range between 1.0 eV and 1.4 eV. Fig. 4(*c*) shows the intensity ratios $I_{L3} = I(a_2)/I(a_1)$ and $I_{L2} = I(b_2)/I(b_1)$ *versus* the hybridization energy parameter $pd\sigma$, both of which decrease as $pd\sigma$ increases. A $pd\sigma$ value between 1.0 eV and 1.4 eV corresponds to $I_{L3} = I(a_2)/I(a_1) \in (1.3, 1.7)$ and $I_{L2} = I(b_2)/I(b_1) \in (1.2, 1.5)$, which is consistent with the $I_{L2}$ value obtained from the experimental spectrum. The experimental $I_{L3}$ value, however, is smaller and falls into the $pd\sigma$ energy range between 1.5 eV and 2 eV. A comprehensive comparison among the energy splitting $\Delta_{L3}$ and $\Delta_{L2}$ values, the intensity ratios $I_{L3}$ and $I_{L2}$, as well as the lineshapes between the $L_3$ and $L_2$ excitation peaks prefers a $pd\sigma$ value in the energy range between 1.0 eV and 1.4 eV; we therefore use $pd\sigma$ = 1.2 eV for our calculations.

We note that different $pd\sigma$ values have been reported for STO compounds in theoretical calculations. Bocquet *et al.* (1996) reported $pd\sigma = 2.6 \pm 0.1$ eV based on the CI cluster model analysis of the core-level metal 2*p* X-ray photoemission spectrum. Haverkort *et al.* (2012) reported a $pd\sigma$ value around 2.3 eV based on *ab initio* multiplet ligand-field theory. This discrepancy might be related to the size of the basis set used and/or the different calculation methods. Our smaller $pd\sigma$ value, however, is consistent with the 1.15 eV reported by Ikeno *et al.* (2009) and by Kroll *et al.* (2015). The early 3*d* transition metal oxide typically shows a large charge transfer energy. The strong covalent effect thus is related to the large hybridization energy. For the STO compound of interest here, the large charge transfer energy and the small hybridization energy resolved by CI cluster calculations suggest a relatively smaller covalent effect in the system than other Ti and V oxides. This is different as suggested by the CI calculation analysis of the STO X-ray photoemission spectrum (Bocquet *et al.*, 1996). Finally, we note that our spectra have been broadened with a Gaussian broadening of 0.15 eV full width at half-maximum (FWHM) and a Lorentzian lifetime broadening with energy-dependent FWHM. The leading peaks, peaks $a_1$, $a_2$, $b_1$ and $b_2$ have FWHM intervals from 0.1 eV to 0.3 eV, 0.3 eV to 0.5 eV, 0.5 eV to 0.7 eV, 0.7 eV to 1.0 eV and 1.0 eV to 1.2 eV, respectively.

### 3.3. Crystal field effects

Accompanying the fast development of thin-film deposition techniques, transition metal thin films and heterostructures have expanded into a booming field. Strain induced by the lattice mismatch between thin film and substrate generally lowers the crystal symmetry from cubic $O_h$ to tetragonal $D_{4h}$. Strain engineering has been proposed to tailor the electronic properties in perovskite thin films and heterostructures (Rondinelli & Fennie, 2012); for example, the enhancement of ferroelectric properties (Haeni *et al.*, 2004), the manipulation of orbital occupancies (Chakhalian *et al.*, 2011; Wu *et al.*, 2013), the modification of octahedral rotations which affect the electric and magnetic properties (Zayak *et al.*, 2006; Rondinelli & Spaldin, 2009), *etc*. We thus consider explicitly a $TiO_6$ octahedron with $D_{4h}$ tetragonal symmetry, to offer theoretical guidance for understanding the experimental $L_{2,3}$-edge X-ray absorption and electron energy-loss spectra based on CI cluster calculations.

A tetragonal distortion generally can be modelled by two additional energy parameters, *i.e.* $\Delta_{t2g}$ and $\Delta_{eg}$, representing the energy splitting of $t_{2g}$ levels [$\Delta_{t2g} = E(d_{yz}, d_{xz}) - E(d_{xy})$] and $e_g$ levels [$\Delta_{eg} = E(d_{3z2-r2}) - E(d_{x2-y2})$], respectively. Fig. 5(*a*) shows the polarization-dependent simulated spectra at different $\Delta_{t2g}$ values ranging from −300 meV to 300 meV. The spectra show strong sensitivities to $\Delta_{t2g}$ and obvious polarization dependence. One might expect that the spectra do not change with different $\Delta_{eg}$ values intuitively since the $e_g$ levels are empty and far away from the antibonding bands near the Fermi level. This, however, is not the case. Different from the $\Delta_{t2g}$-dependent spectra where the excitations to $t_{2g}$ levels are activated (peak $a_1$ and $b_1$), the peaks $a_2$ and $b_2$ with corresponding excitations to $e_g$ levels show considerable linear dichroic effects with different $\Delta_{eg}$ values, as shown in Fig. 5(*b*), which we attribute to a change of the final states as $\Delta_{eg}$ varies.

Fig. 5(*c*) shows the normalized dichroic spectra for negative and positive $\Delta_{t2g}$ values, where the signs and magnitudes of the natural linear dichroism change substantially. The leading peaks exhibit strong natural dichroism due to the intrinsic

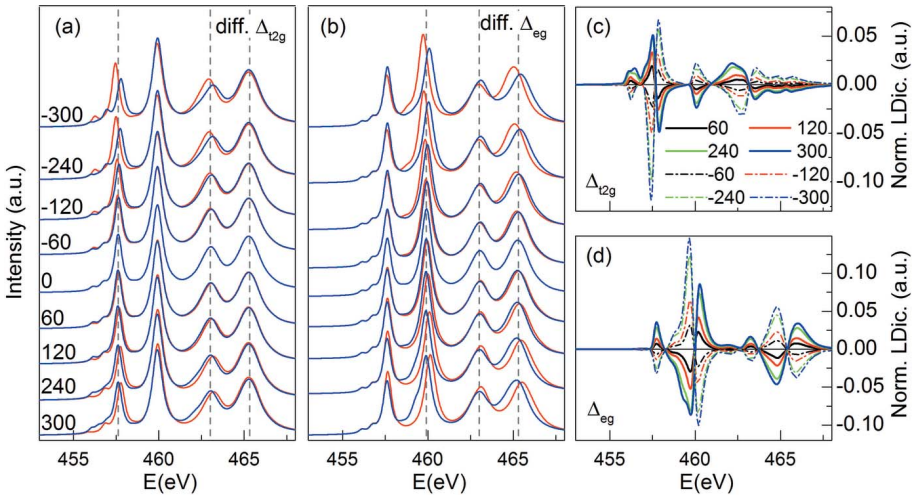


**Figure 5**
(*a*, *b*) Calculated soft X-ray absorption spectra for a $TiO_6$ cluster with photon polarization parallel ($E \parallel c$) and perpendicular ($E \perp c$) to the crystal *c*-axis at different $\Delta_{t2g}$ values and different $\Delta_{eg}$ values, *i.e.* −300, −240, −120, −60, 0, 60, 120, 240 and 300 meV from top to bottom spectra. The crystal field splitting value is shown beside the corresponding plot in units of meV. (*c*, *d*) Normalized linear dichroic spectra, *i.e.* $(XAS_{E\perp,c} - XAS_{E\parallel c})/[(2I_x + I_z)/3]$ for different $\Delta_{t2g}$ and $\Delta_{eg}$ values.

predominantly triplet characters which are mixed into the main $L_3$ set of peaks through spin–orbit interactions and Coulomb repulsion interactions (de Groot *et al.*, 1990). The two linear dichroic spectra, although showing opposite signs to each other, are not interchangeable simply by reversing their respective signs which is related to the complicated multiplet effects. Fig. 5(*d*) shows the normalized dichroic spectra calculated at different $\Delta_{eg}$ values. The linear dichroic spectra are almost symmetric for positive and negative $\Delta_{eg}$ values, consistent with the isotropic nature of the $e_g$ orbitals when $\Delta_{eg}$ varies.

We further calculate the spectra with both $\Delta_{t2g}$ and $\Delta_{eg}$ energy parameters. In principle, any $\Delta_{t2g}$ and $\Delta_{eg}$ values can be used to parameterize the different spectra, depending on the details of the $TiO_6$ octahedral distortion. For instance, an expansion of the out-of-plane Ti—O bond length and a compression of the Ti—O in-plane bond length results in decreased/increased Ti—O overlapping, which could happen when STO thin films are under compressive strain. The different hybridization strengths between $e_g$ and $t_{2g}$ orbitals are essentially attributed to the $e_g$ orbitals pointing towards the nearest O *p* orbitals. The hopping magnitude of the $e_g$–O *p* orbitals is twice as large as that of the $t_{2g}$–O *p* orbitals as mentioned above. We thus took the value of $\Delta_{eg}$ as $2\Delta_{t2g}$ in our calculations in the first approximation, considering only the anisotropic hybridization strength.

Fig. 6(*a*) shows the polarization-dependent simulated spectra at different $\Delta_{t2g}$ and $\Delta_{eg}$ values. The opposite dichroic effects appear at very small positive and negative crystal field values, which can be related to the insulating nature of the STO compound. This is different from metallic systems, where the considerable bandwidth should be taken into account. A clear energy shift, *i.e.* a band splitting of the $t_{2g}$ and $e_g$ sub-levels, has been observed for the spectra with both positive and negative $\Delta_{t2g}$ and $\Delta_{eg}$ values. We denote the energy shift as the spectra splitting between photons with parallel ($E \parallel c$) and perpendicular ($E \perp c$) polarizations. The positive (negative) energy shift indicates that the $d_{xy}$ ($d_{xz}$, $d_{yz}$) and the $d_{x2-y2}$ ($d_{3z2-r2}$) orbitals are lower in energy. The energy shifts for both $t_{2g}$-excited ($a_1$ and $b_1$) peaks and $e_g$-excited ($a_2$ and $b_2$) peaks are opposite in response to the positive and negative $\Delta_{t2g}$ and $\Delta_{eg}$ values but do not show a linear dependence. The simulated spectra show larger energy shifts for negative crystal field splitting, suggesting that compressive strain is a more efficient parameter for manipulating the orbital engineering of STO-based thin films.

We further compare the energy shifts calculated by taking both $\Delta_{t2g}$ and $\Delta_{eg}$ values into account and the energy shifts calculated considering only $\Delta_{t2g}$ or $\Delta_{eg}$ separately. Fig. 6(*b*) shows the averaged energy shift of peak $a_1$ and $b_1$ between the spectra calculated considering both $\Delta_{t2g}$ and $\Delta_{eg}$ values and the spectra calculated with $\Delta_{t2g}$ alone. The energy splits of $t_{2g}$-excited peaks are not equal in both cases, whereas the energy shifts of $e_g$-excited peaks for the $\Delta_{eg}$ case are comparable [as shown in Fig. 6(*c*)]. This observation indicates that a proper understanding of the experimentally resolved orbital selective energy shifts should include the $e_g$ crystal field splitting, even

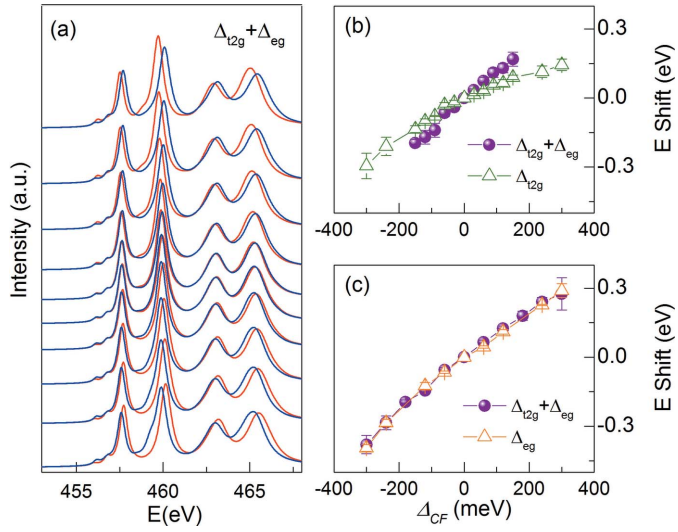


**Figure 6**
(*a*) Calculated soft X-ray absorption spectra for $E \parallel c$ and $E \perp c$ photon polarizations at different crystal field splitting values, *i.e.* $\Delta_{t2g}$ of −150, −120, −90, −60, −30, 30, 60, 90, 120 and 150 meV from top to bottom spectra and $\Delta_{eg} = 2\Delta_{t2g}$. (*b*) Comparison of averaged energy shift of peak $a_1$ and $b_1$ for ($E \parallel c$) and ($E \perp c$) polarizations between the spectra calculated considering both $\Delta_{t2g}$ and $\Delta_{eg}$ values and the spectra calculated considering only the splitting of $t_{2g}$ levels, *i.e.* $\Delta_{t2g}$. (*c*) Comparison of averaged energy shift of peak $a_2$ and $b_2$ between the spectra calculated for both $\Delta_{t2g}$ and $\Delta_{eg}$ values and the spectra calculated considering only $\Delta_{eg}$.

though the $e_g$ orbitals are not relevant for the local ground state properties, at least in the STO-related thin films investigated here.

## 4. Conclusion

In summary, we carried out CI cluster calculations for a $TiO_6$ octahedron of STO compound, which can reproduce well the experimentally measured $L_{2,3}$-edges absorption spectrum. Detailed investigations between the experimental spectrum and the simulated spectra yield the values of different energy parameters, *e.g.* a correction of 70–80% of the Slater parameters needs to be considered for inclusion of intra-atomic interactions. The energy splitting of the $L_{2,3}$ set of peaks in the X-ray absorption spectrum is not equal to the crystal field splitting energy $10Dq$ with $O_h$ symmetry directly, which, however, can be obtained through CI calculations, *i.e.* $10Dq$ = 1.8–2 eV for STO oxide. Different $pd\sigma$ values had been reported for STO compounds in other theoretical calculations where the discrepancy might be related to the size of the basis set used and/or the different calculation methods. Our careful analyses of the energy splitting $\Delta_{L3,L2}$ values and the peak intensity ratios quantitatively, taking the lineshapes of the $L_3$ and $L_2$ excitation peaks into account, yield $pd\sigma$ = 1.2 eV, indicative of a smaller covalent effect of STO compound compared with other Ti oxides, *e.g.* $TiO_2$ and $LaTiO_3$ compounds. We finally emphasize the photon polarization-dependent absorption spectra with different tetragonal crystal field splitting. For symmetry reasons, the spectra show dramatic natural linear dichroism. The energy shifts do not show linear dependences in response to the positive and negative $\Delta_{t2g}$ and $\Delta_{eg}$ values. The larger energy shifts for negative crystal field splitting suggests that compressive strain is a more efficient parameter for manipulating the orbital engineering of STO-based thin films. A detailed investigation of the energy shifts in different $\Delta_{t2g}$ and $\Delta_{eg}$ crystal fields suggests that a thorough understanding of the experimentally resolved energy shifts should include the $e_g$ crystal field splitting, even though the $e_g$ orbitals are not relevant for the local ground state properties. Our simulations show the powerful features of CI cluster calculations and its potential in understanding the full absorption spectra.

## Acknowledgements

We acknowledge the valuable discussions with M. W. Haverkort, X. P. Yang, and the provision of synchrotron radiation beam time at the 4B9B beamline of the Beijing Synchrotron Radiation Facility.

## Funding information

Funding for this research was provided by: National Natural Science Foundation of China (grant No. 11704317; grant No. U1332105); China Postdoctoral Science Foundation (grant No. 2016M602064); Fundamental Research Funds for Central Universities (grant No. 20720160020); Center for Functional Nanomaterials, which is a US DOE Office of Science Facility, at Brookhaven National Laboratory (contract No. DE-SC0012704l to HLX).

## References

Arenholz, E., van der Laan, G., Fraile-Rodríguez, A., Yu, P., He, Q. & Ramesh, R. (2010). *Phys. Rev. B*, **82**, 140103.
Bocquet, A. E., Mizokawa, T., Morikawa, K., Fujimori, A., Barman, S. R., Maiti, K., Sarma, D. D., Tokura, Y. & Onoda, M. (1996). *Phys. Rev. B*, **53**, 1161–1170.
Bunău, O. & Joly, Y. (2012). *Phys. Rev. B*, **85**, 155121.
Cen, C., Thiel, S., Mannhart, J. & Levy, J. (2009). *Science*, **323**, 1026–1030.
Chakhalian, J., Rondinelli, J. M., Liu, J., Gray, B. A., Kareev, M., Moon, E. J., Prasai, N., Cohn, J. L., Varela, M., Tung, I. C., Bedzyk, M. J., Altendorf, S. G., Strigari, F., Dabrowski, B., Tjeng, L. H., Ryan, P. J. & Freeland, J. W. (2011). *Phys. Rev. Lett.* **107**, 116805.
Choi, T., Lee, S., Choi, Y. J., Kiryukhin, V. & Cheong, S.-W. (2009). *Science*, **324**, 63–66.
Comes, R. B., Xu, P., Jalan, B. & Chambers, S. A. (2015). *Appl. Phys. Lett.* **107**, 131601.
Dawber, M., Rabe, K. M. & Scott, J. F. (2005). *Rev. Mod. Phys.* **77**, 1083–1130.
Fronzoni, G., De Francesco, R. & Stener, M. (2012). *J. Chem. Phys.* **137**, 224308.
Gilmore, K., Vinson, J., Shirley, E., Prendergast, D., Pemmaraju, C., Kas, J., Vila, F. & Rehr, J. (2015). *Comput. Phys. Commun.* **197**, 109–117.
Groot, F. M. F. de, Fuggle, J. C., Thole, B. T. & Sawatzky, G. A. (1990). *Phys. Rev. B*, **41**, 928–937.
Haeni, J. H., Irvin, P., Chang, W., Uecker, R., Reiche, P., Li, Y. L., Choudhury, S., Tian, W., Hawley, M. E., Craigo, B., Tagantsev, A. K., Pan, X. Q., Streiffer, S. K., Chen, L. Q., Kirchoefer, S. W., Levy, J. & Schlom, D. G. (2004). *Nature (London)*, **430**, 758–761.
Haverkort, M. W. (2016). *Quanty – a quantum many-body script language*, http://www.quanty.org/.
Haverkort, M. W., Zwierzycki, M. & Andersen, O. K. (2012). *Phys. Rev. B*, **85**, 165113.
Hwang, H. Y., Iwasa, Y., Kawasaki, M., Keimer, B., Nagaosa, N. & Tokura, Y. (2012). *Nat. Mater.* **11**, 103–113.
Ikeno, H., de Groot, F. M. F., Stavitski, E. & Tanaka, I. (2009). *J. Phys. Condens. Matter*, **21**, 104208.
Kroll, T., Solomon, E. I. & de Groot, F. M. F. (2015). *J. Phys. Chem. B*, **119**, 13852–13858.
Krüger, P. (2010). *Phys. Rev. B*, **81**, 125121.
Krüger, P. & Natoli, C. R. (2016). *J. Phys. Conf. Ser.* **712**, 012007.
Laan, G. van der, Westra, C., Haas, C. & Sawatzky, G. A. (1981). *Phys. Rev. B*, **23**, 4369–4380.
Laan, G. van der, Zaanen, J., Sawatzky, G. A., Karnatak, R. & Esteva, J.-M. (1986). *Phys. Rev. B*, **33**, 4253–4263.
Laskowski, R. & Blaha, P. (2010). *Phys. Rev. B*, **82**, 205104.
Maganas, D., DeBeer, S. & Neese, F. (2014). *Inorg. Chem.* **53**, 6374–6385.
Marschall, R. (2014). *Adv. Funct. Mater.* **24**, 2421–2440.
Ohtomo, A. & Hwang, H. Y. (2004). *Nature (London)*, **427**, 423–426.
Okada, K., Uozumi, T. & Kotani, A. (1994). *J. Phys. Soc. Jpn*, **63**, 3176–3184.
Ootsuki, S., Ikeno, H., Umeda, Y., Yonezawa, Y., Moriwake, H., Kuwabara, A., Kido, O., Ueda, S., Tanaka, I., Fujikawa, Y. & Mizoguchi, T. (2014). *Microscopy*, **63**, 249–254.
Ramanantoanina, H. & Daul, C. (2017). *Phys. Chem. Chem. Phys.* **19**, 20919–20929.
Reyren, N., Thiel, S., Caviglia, A. D., Kourkoutis, L. F., Hammerl, G., Richter, C., Schneider, C. W., Kopp, T., Rüetschi, A.-S., Jaccard, D., Gabay, M., Muller, D. A., Triscone, J.-M. & Mannhart, J. (2007). *Science*, **317**, 1196–1199.
Rondinelli, J. M. & Fennie, C. J. (2012). *Adv. Mater.* **24**, 1918.
Rondinelli, J. M. & Spaldin, N. A. (2009). *Phys. Rev. B*, **79**, 054409.

Schlom, D. G., Chen, L.-Q., Eom, C.-B., Rabe, K. M., Streiffer, S. K. & Triscone, J.-M. (2007). *Annu. Rev. Mater. Res.* **37**, 589–626.
Slater, J. C. & Koster, G. F. (1954). *Phys. Rev.* **94**, 1498–1524.
Tanaka, A. & Jo, T. (1994). *J. Phys. Soc. Jpn*, **63**, 2788–2807.
Torres-Pardo, A., Gloter, A., Zubko, P., Jecklin, N., Lichtensteiger, C., Colliex, C., Triscone, J.-M. & Stéphan, O. (2011). *Phys. Rev. B*, **84**, 220102.
Uehara, Y., Lindle, D., Callcott, T., Terminello, L., Himpsel, F., Ederer, D., Underwood, J. H., Gullikson, E. M. & Perera, R. (1997). *Appl. Phys. A*, **65**, 179–182.
Vinson, J., Rehr, J. J., Kas, J. J. & Shirley, E. L. (2011). *Phys. Rev. B*, **83**, 115106.
Woicik, J. C., Shirley, E. L., Hellberg, C. S., Andersen, K. E., Sambasivan, S., Fischer, D. A., Chapman, B. D., Stern, E. A., Ryan, P., Ederer, D. L. & Li, H. (2007). *Phys. Rev. B*, **75**, 140103.
Wu, M., Benckiser, E., Haverkort, M. W., Frano, A., Lu, Y., Nwankwo, U., Brück, S., Audehm, P., Goering, E., Macke, S., Hinkov, V., Wochner, P., Christiani, G., Heinze, S., Logvenov, G., Habermeier, H.-U. & Keimer, B. (2013). *Phys. Rev. B*, **88**, 125124.
Wu, M., Zheng, J.-C. & Wang, H.-Q. (2017). *J. Appl. Cryst.* **50**, 576–584.
Zayak, A. T., Huang, X., Neaton, J. B. & Rabe, K. M. (2006). *Phys. Rev. B*, **74**, 094104.